Rapid biogenesis and sensitization of secretory lysosomes in NK cells mediated by target-cell recognition

Dongfang Liu*†‡, Liang Xu*‡, Fan Yang*, Dongdong Li*, Feili Gong†§, and Tao Xu*§¶

¶National Laboratory of Biomacromolecules, Institute of Biophysics, Chinese Academy of Sciences, Beijing 100101, China; and *Institute of Biophysics and Biochemistry, School of Life Science and Technology, and †Institute of Immunology, Tongji Medical College, Huazhong University of Science and Technology, Wuhan 430074, China

Edited by William S. Sly, Saint Louis University School of Medicine, St. Louis, MO, and approved November 11, 2004 (received for review August 5, 2004)

Natural killer (NK) cells play important roles in defense against tumor, viral infection, and cell-mediated xenograft rejection through secretion of secretory lysosomes. In this study, we used high time-resolution membrane capacitance measurement and fluorescence-imaging techniques to study the biogenesis and exocytosis of secretory lysosomes in a human NK cell line. We demonstrated a high-affinity Ca^{2+}-dependent exocytosis of secretory lysosomes, which is sensitized further after target-cell stimulation. Our data also suggest an unusual rapid and dramatic *de novo* formation of secretory lysosomes after target-cell recognition. The rapid biogenesis of secretory lysosomes was blocked by specific protein kinase C inhibitor but not by brefeldin A. We propose that target-cell recognition triggers rapid biogenesis and sensitization of secretory lysosomes in NK cells through activation of PKC.

exocytosis | lytic granules | calcium | immune defense

Natural killer (NK) cells and cytotoxic T lymphocytes play critical roles in the innate immune system and are crucial in defense against tumor and viral infection. These cells are furnished with the so-called lytic granules, which contain an array of cytotoxic and proteolytic molecules such as perforin, granzymes, and granulysin (1). After receptor recognition of susceptible targets, subsequent Ca^{2+}-dependent exocytosis of the lytic granules leads to rapid lysis of the target cells (1). In contrast to most secretory cells, which store their secretory products in specialized secretory granules, NK cells store their secretory proteins in the lytic granules, a dual-function organelle recently regarded as secretory lysosomes (SLs). SLs are unusual in that they serve both as a degradative and a secretory pathway. Despite extensive studies conducted on the exocytosis of secretory granules from endocrine and neuronal cells (2), little is known about the properties and regulation of the SLs in NK cells. It is unclear how different the processes that underlie the secretion of SLs and secretory granules are. The strongest evidence that they differ comes from the existence of genetic diseases that selectively affect SL function without apparently affecting the secretory granules (3).

The ability of NK cells and T lymphocytes to kill depends on the activation state of the cells. Resting T lymphocytes do not possess SLs (4). Activation after T cell receptor recognition triggers the biogenesis of electron-dense SLs (5, 6). NK cells, on the other hand, are capable of destroying target cells without prior sensitization through exocytosis of preformed SLs (6). However, it is unclear whether the preformed SLs are sufficient, or the *de novo* formation of SLs is necessary, for their lytic function. In addition, the mechanisms involved in the biogenesis of SLs remain poorly understood. Both the endosomal route and direct transportation from vesicles originating in the trans-Golgi network (TGN) have been suggested for the biogenesis of SLs. This feature is different from the formation of the regulated secretory granules, which involves primarily budding from the TGN and subsequent maturation.

In light of the importance of NK cells in innate immune defense, it is desirable to characterize the biogenesis, maturation, and exocytosis of SLs in these cells and to unravel the underlying mechanisms. To this end, we studied the characteristics of exocytosis and rapid biogenesis of SLs from an NK cell line (NK92) by using high time-resolution membrane capacitance (C_m) measurement, a Ca^{2+} flash-photolysis technique, and deconvolution fluorescence microscopy.

Materials and Methods

Cell Culture and Solutions. NK92 cells were cultured in α-MEM medium supplemented with 12.5% calf serum, 12.5% horse serum, and 100 units/ml recombinant human IL-2. Primary porcine endothelial cells (PECs) were cultured in M199 medium supplemented with 15% calf serum. In the NK92 and PEC conjugation assay, the PECs were cultured onto a glass coverslip, and then NK cells were dropped onto the PECs for ≈10 min before electrical recordings or image collection.

SLs of NK cells were labeled by incubating the cells in external solution containing 3 μM acridine orange (AO) (Molecular Probes) for 10 min, and then cells were washed twice by dye-free external solution. To activate or inhibit protein kinase C (PKC), AO-labeled NK cells were incubated in external solution containing 100 nM phorbol 12-myristate 13-acetate (PMA) for 5 min or 100 nM Gö6983 (Calbiochem) for 30 min before image collection. Incubation in external solution containing 10 mg/liter brefeldin A (BFA) for 40 min was used to block Golgi budding. Stock solutions of PMA and Gö6983 were prepared in DMSO. The final concentration of DMSO in diluted solutions was $<0.02\%$. All experiments were performed at room temperature.

The external solution contained 145 mM NaCl, 5 mM KCl, 1 mM $MgCl_2$, 2 mM $CaCl_2$, 10 mM Hepes, and 5 mM glucose. For C_m recording, the standard pipette solution contained 125 mM K-glutamate, 10 mM NaCl, 2 mM MgATP, and 10 mM Hepes. Pipette solutions with different Ca^{2+} concentrations were made from the standard pipette solution by adding 10 mM *N*-(2-hydroxyethyl)ethylenediamine-*N*,*N*′,*N*′-triacetic acid (K_d = 3.96 μM for Ca^{2+} at pH 7.2) and the proper concentration of $CaCl_2$. The caged-Ca^{2+}-containing internal solutions consisted of 110 mM Cs-glutamate, 5 mM 1-(2-nitro-4,5-dimethoxyphenyl)-*N*,*N*,*N*′,*N*′-tetrakis[(oxycarbonyl)methyl]-1,2-ethanediamine, 4 mM $CaCl_2$, 2 mM MgATP, 0.3 mM GTP, 0.2 mM 2-[2-(5-carboxy)oxazole]-5-hydroxy-6-aminobenzofuran-*N*,*N*,*O*-triace-

This paper was submitted directly (Track II) to the PNAS office.

Abbreviations: NK, natural killer; SL, secretory lysosome; TGN, trans-Golgi network; C_m, membrane capacitance; PEC, porcine endothelial cell; AO, acridine orange; PKC, protein kinase C; PMA, phorbol 12-myristate 13-acetate; BFA, brefeldin A; G_m, membrane conductance; G_s, series conductance; RRP, readily releasable pool; SRP, slowly releasable pool; FWHM, full width at half maximum.

‡D.L. and L.X. contributed equally to this work.

§To whom correspondence may be addressed. E-mail: flgong@163.com or xutao@ibp.ac.cn.

tic acid, and 35 mM Hepes. The basal $[Ca^{2+}]_i$ was measured to be ≈200 nM by fura-2. The pipette solution was adjusted to pH 7.2 by either HCl or CsOH. All reagents were purchased from Sigma unless otherwise stated.

Capacitance Measurement. Conventional whole-cell patch-clamp measurements were performed by using an EPC-9 patch-clamp amplifier and PULSE software (HEKA, Lambrecht, Germany). Capacitance measurements were performed by using the "sine+dc" software lock-in amplifier method implemented in the PULSE software. A sinusoid voltage stimulation (1,000 Hz with an amplitude of 40 mV) was superimposed on a holding potential of −60 mV. Only recordings that fulfilled the following criteria were included in the analysis: (*i*) membrane conductance (G_m) < 1 nS and minimum series conductance (G_s) > 50 nS; (*ii*) the recording duration was >300 s; and (*iii*) the changes in C_m did not accompany concurrent changes in G_s or G_m.

Flash-Photolysis and $[Ca^{2+}]_i$ Measurement. Flashes of UV light and fluorescence excitation light were generated as described by Xu *et al*. (7). $[Ca^{2+}]_i$ of individual cells was monitored with a photomultiplier-based system by using a monochromatic light source (TILL Photonics, Gräfelting, Germany) tuned to excite 2-[2-(5-carboxy)oxazole]-5-hydroxy-6-aminobenzofuran-*N*,*N*,*O*-triacetic acid fluorescence at 345 and 385 nm. $[Ca^{2+}]_i$ was calculated from the fluorescence ratio *R* according to Grynkiewicz *et al*. (8). To obtain stepwise $[Ca^{2+}]_i$ increases, short flashes of UV light from a xenon arc flash lamp (Rapp OptoElectronics, Hamburg, Germany) were applied to the whole cell loaded with caged Ca^{2+}.

Image Collection. Cells were grown on high-refractive-index glass coverslips ($n = 1.78$) and viewed with a fluorescence microscope system as described (9). We took advantage of the high-numeric-aperture objective (APO × 100 OHR, numeric aperture of 1.65, Olympus, Melville, NY) to take high-resolution fluorescence images of AO load cells. A series of 2D images was collected by moving the focal plane with the piezoelectric *z*-axis scanning controller (E-662. LR; Physik Instruments, Karlsruhe, Germany). Accordingly, those 2D section images were used to reconstruct 3D images of the cell. The iterative expectation-maximum algorithm based on a maximum-likelihood approach (10) was used to deconvolve the recorded fluorescence image. The deconvolution algorithm used in our study was regularized with intensity regularization to avoid the appearance of artifacts (10). MATLAB 6.5 (Mathworks, Natick, MA) was used for deconvolution and 3D reconstruction. Spots were counted as SLs if the average intensity in the central 9 × 9-pixel region exceeded five times the SD noise of intracellular background. Total internal reflection fluorescence microscopy setup was constructed on the basis of prismless and through-the-lens configuration as described (9).

The emission spectrum of AO depends on pH. AO produces a bright-orange to red color depending on pH. The fluorescence of AO was excited at 488 nm and collected through a dual-view MicroImager (Optical Insights, Santa Fe, NM), which enables simultaneous fluorescence collection at 520 ± 15-nm (green) and 630 ± 25-nm (red) emission. The pH of each spot was estimated by calculating the fluorescence ratio of the red-to-green emission. Calibration of the fluorescence ratio with pH *in situ* was accomplished with a mix of the alkali cation/H^+ ionophores nigericin and monensin in bath solutions of defined pH as described (11).

Statistical Analysis. Data analysis was carried out by using IGOR PRO software (Wavemetrics, Lake Oswego, OR). Averaged results are expressed as mean ± SEM. Comparisons between means were performed by using Student's *t* test. Double asterisks indicate $P < 0.01$ in Figs. 2 and 4.

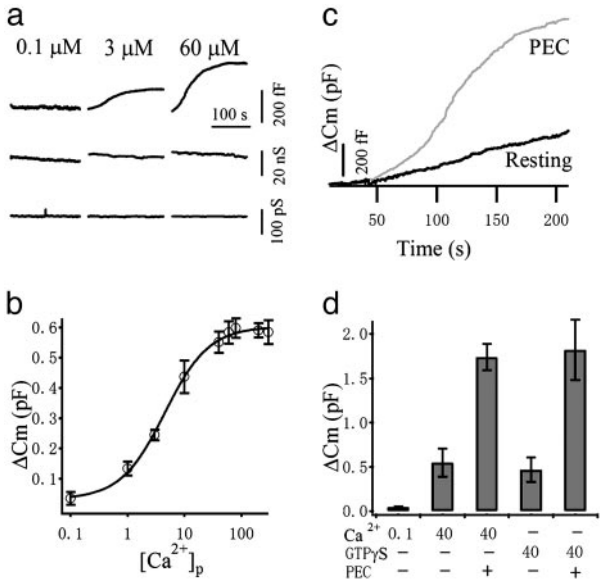

Fig. 1. Calcium-dependent exocytosis in NK cells. (*a*) Example traces of C_m increase (ΔC_m), G_s, and G_m from three cells patched with 0.1, 3, and 60 μM free Ca^{2+} in the pipette solution ($[Ca^{2+}]_p$), respectively. (*b*) The averaged total ΔC_m values are plotted against $[Ca^{2+}]_p$ (n = 13–23). The line represents a fit using a logistic equation, which gives an EC_{50} of 4.5 μM. (*c*) Example ΔC_m traces from resting and PEC-activated NK cells demonstrating dramatic augmentation of the secretory response after PEC stimulation. (*d*) The mean ± SEM values (n = 11–27) from resting cells recorded with 0.1 and 40 μM $[Ca^{2+}]_p$ and 40 μM GTPγS are compared with that of PEC-activated NK cells stimulated with 40 μM $[Ca^{2+}]_p$ and 40 μM GTPγS.

Results and Discussion

A common feature of exocytosis in many cellular systems is its activation by cytosolic Ca^{2+}. We used C_m measurement to monitor exocytosis in human NK92 cells at millisecond time resolution (12). The human NK92 cell line has been used as a favorable tool in the functional study of NK cells and in immunotherapy (13). Highly Ca^{2+}-buffered pipette solutions with different Ca^{2+} concentrations ($[Ca^{2+}]_p$) were dialyzed against the cytosol in standard whole-cell patch-clamp mode. Fig. 1*a* displays typical recordings from three different cells microperfused with different $[Ca^{2+}]_p$. No obvious increase in C_m could be observed at low $[Ca^{2+}]_p$ (<100 nM). However, at higher $[Ca^{2+}]_p$, a small amount of monophasic C_m increment (ΔC_m) could be elicited. To examine the Ca^{2+} dependence of secretion, we plotted the averaged ΔC_m against $[Ca^{2+}]_p$ in Fig. 1*b*. The plot is fitted with a logistic equation, which yields $EC_{50} \approx 4.5$ μM, suggesting a rather high affinity for Ca^{2+}. It has been shown in hematopoietic cells such as mast cells and neutrophils that complete degranulation can be induced by intracellular perfusion of GTPγS (14–16). We also tested whether GTPγS is effective in inducing degranulation in NK cells. As shown in Fig. 1*d*, GTPγS at 40 μM triggered a ΔC_m of 471 ± 142 (n = 11) fF, not very different from the maximal ΔC_m induced by Ca^{2+}.

NK cells are thought to destroy target cells through exocytosis of preformed lytic granules without prior sensitization (6). Consistent with this idea, we have demonstrated a small Ca^{2+}-dependent exocytosis in resting NK cells. However, the amount of exocytosis in resting NK cells is much less compared with other haemopoietic cells such as mast cells and neutrophils. At maximal stimulation of Ca^{2+} concentration, the averaged ΔC_m from resting NK cells is only 598 ± 32 fF (n = 13), corresponding

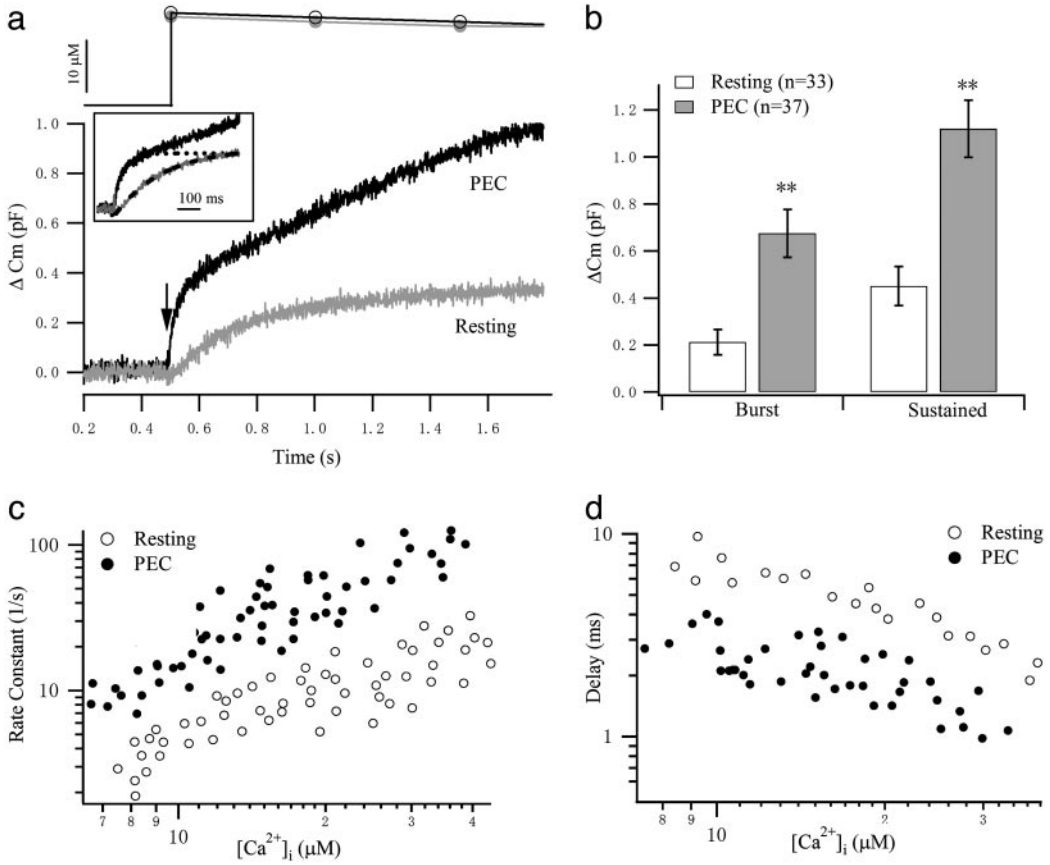

Fig. 2. Kinetics of exocytosis in response to flash photolysis of caged Ca^{2+}. (*a*) Comparison of the C_m responses to a similar postflash $[Ca^{2+}]_i$ level from resting and PEC-activated NK cells. (*Inset*) The exocytotic bursts are normalized, expanded, and compared. Dashed lines represent single exponential fits to the burst component. (*b*) The amplitudes of the exocytotic burst and the sustained components were estimated from the exponential fit and are compared between resting ($n = 37$) and PEC-activated ($n = 33$) NK cells. **, $P < 0.01$. (*c*) Rate constants for resting (open circles) and PEC-activated (filled circles) cells are plotted against postflash $[Ca^{2+}]_i$ levels. (*d*) The delay between the flash and the start of fusion is plotted against postflash $[Ca^{2+}]_i$ levels.

to 76 SLs, assuming an average diameter of 500 nm (17), and a specific C_m as 10 fF/μm (2, 18), whereas for mast cells and neutrophils, the estimated granule number is >1,000 (15, 16, 19). It is unclear whether the preformed SLs are sufficient or the *de novo* formation of SLs is necessary for their lytic function. PECs have been widely used to activate xenogeneic NK cytotoxicity (20). When NK cells were allowed to drop onto a monolayer of PECs for 10 min, we observed a large augmentation in the secretory response elicited by Ca^{2+}, as shown in Fig. 1*c*. At the same $[Ca^{2+}]_p$ of 40 μM, ΔC_m increased from 551 ± 35 fF ($n = 21$) to 1,742 ± 213 fF ($n = 17$) after PEC activation, demonstrating a 3.2-fold increase. Interestingly, PEC treatment also augmented the GTPγS-induced exocytosis to a similar extent (Fig. 1*d*), suggesting that the large augmentation in degranulation after PEC interaction is not initiated through activation of a GTP-binding protein.

The existence of different maturation states of vesicles results in different kinetic components of exocytosis after prolonged stimulation: an initial, rapid exocytotic burst, which happens on a tens-of-milliseconds scale in chromaffin cells, is followed by a slower, sustained phase (21, 22). Detailed analysis of the exocytotic burst in response to flash photorelease of Ca^{2+} from chromaffin cells has revealed a sum of two exponential components, indicating the presence of two releasable vesicle pools with distinct release kinetics. These vesicle pools have been termed the "readily releasable pool" (RRP) and the "slowly releasable pool" (SRP) (22, 23). The existence of the releasable pools of vesicles in synapse and endocrine cells is thought to be important for assuring their prompt stimulus-secretion coupling required for their physiological functions. It is unclear whether a predocked and releasable pool of SLs in NK cells exists. To our surprise, we observed an initial exocytotic burst with a single time constant of ≈200 ms around 20 μM $[Ca^{2+}]_i$ in resting NK cells (Fig. 2 *a* and *c*). The kinetics of this burst is similar to that of the SRP but slower than that of the RRP in chromaffin cells. PEC stimulation dramatically increased both the burst and sustained component (Fig. 2*b*). We further analyzed the relationship between Ca^{2+} and the rate constant of exocytosis of the burst component. The rate constants were obtained by fitting the exocytotic burst with single exponential and displayed versus $[Ca^{2+}]_i$ (Fig. 2*c*). According to the multiple Ca^{2+}-binding model of exocytosis, the rate of exocytosis is proportional to the power of $[Ca^{2+}]_i$ at lower $[Ca^{2+}]_i$ levels (24). The power dependence of the rate constants on $[Ca^{2+}]_i$ at lower $[Ca^{2+}]_i$ (<15 μM) was estimated to be 1.86 with a 95.4% confidence interval of 0.74, suggesting that the triggering of exocytosis in NK cells possibly requires binding of two to three Ca^{2+} ions. By contrast, the peroxidase-positive primary granules in human neutrophils were suggested to have a very low affinity for Ca^{2+} (EC_{50} of 100 μM) with a striking slope factor of 6–15 (16).

PEC stimulation not only increased the RRP size but also enabled the readily releasable SLs to secrete at a much higher rate, as demonstrated in Fig. 2 *a* and *c*. Along with this effect, the delay between the flash and the start of fusion is shortened after PEC stimulation (Fig. 2*d*). Thus, it seems that the burst component has been transformed from an SRP to an RRP after

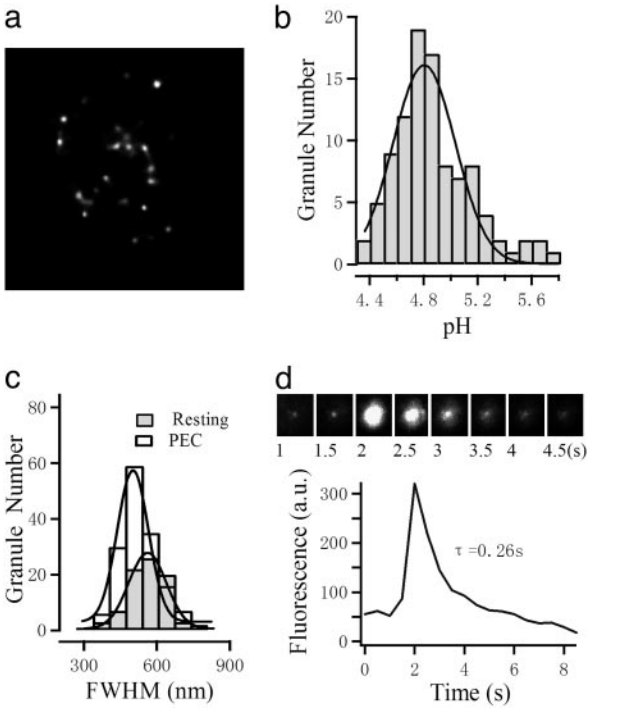

Fig. 3. AO-labeled SLs in NK cells. (*a*) An example section of an AO-stained NK cell after PEC activation. Fluorescence spots are clearly distinguishable. (Scale bar, 5 μm.) (*b*) The pH values of individual granules were determined, and their distribution demonstrates a single peak at 4.8. (*c*) The distributions of the FWHM of spots from resting (filled bar) and PEC-activated (open bar) NK cells are compared. Solid lines represent respective Gaussian fits. The FWHMs were measured from the fluorescence profile of individual spots, which also follow a Gaussian equation. (*d*) Fusion of a single AO-labeled spot revealed by total internal reflection fluorescence microscopy imaging.

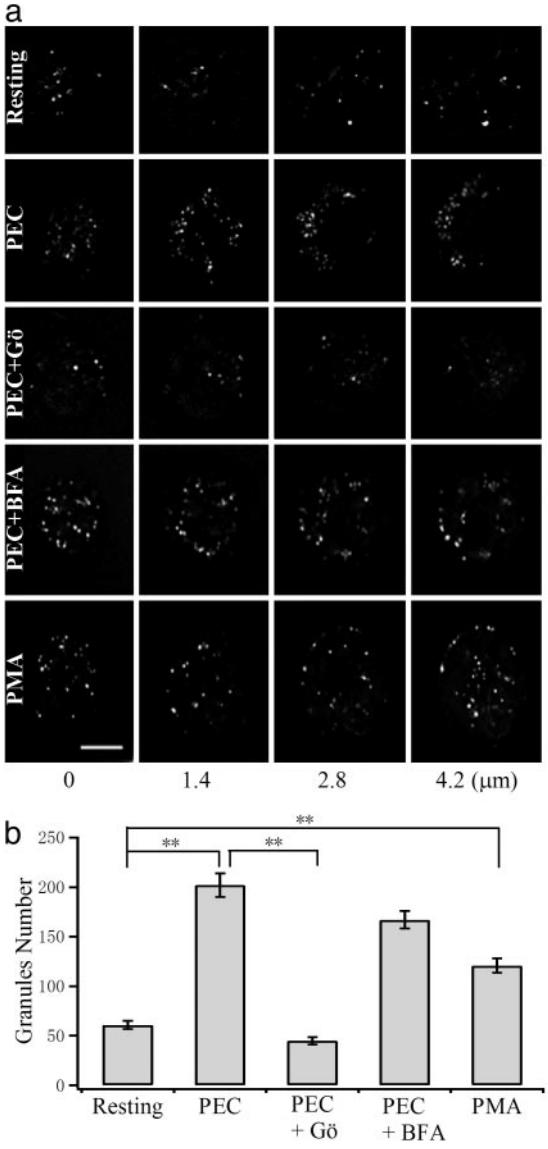

Fig. 4. PEC stimulation increases the number of SLs. (*a*) Four different sections of AO-stained NK cells. The images were deconvolved to better resolve the AO-labeled SLs. Shown from top to bottom are resting, PEC-activated, and PEC+Gö- (Gö6983), PEC+BFA-, and PMA-treated NK cells. (Scale bar, 5 μm.) (*b*) Comparison of the total number of SLs under different conditions as those described for *a*. **, $P < 0.01$.

target-cell recognition, which might be a consequence of sensitization of the Ca^{2+} sensor for exocytosis. The sensitization of the fusion machinery of SLs may facilitate the release of lytic contents in the killing process at subsided $[Ca^{2+}]_i$. It is worth noting that, compared with the RRP of chromaffin cells and β cells (2), although the burst component after PEC conjunction has similar rate constants, it consistently has a significantly shorter delay. This result suggests that SLs might use a different Ca^{2+}-sensitive fusion machinery from that of secretory granules.

The augmentation of exocytotic response by PEC stimulation could be caused by either a shift of SLs from an unreleasable state to a releasable state or an increase in the total number through rapid genesis of nascent SLs. To test for this possibility, we used AO to label the SLs and visualized them under fluorescence microscope. AO produces a pale-green staining at neutral pH. When it accumulates within acidic vesicles, it produces a bright-orange to red color (25). After AO staining, we observed punctate fluorescence, as exemplified in Fig. 3*c*. The color of the fluorescence spots were red, and we found that the pH of these spots follow a Gaussian distribution peaked at 4.8 (Fig. 3*b*), correlating well with the acidic nature of SLs (26). The fluorescence spots exhibit a Gaussian fluorescence profile. We measured the full width at half maximum (FWHM) as an indicator of the granule size. The histogram of FWHM is shown in Fig. 3*c*. The distribution of FWHM could be fitted with a Gaussian function peaked at 523 ± 9.7 nm in resting NK cells, which is slightly larger than that of PEC-activated NK cells (494 ± 7.2 nm). The peak FWHM of the spots corresponds well with the reported size of lytic granules in NK cells (26). To further verify the labeling of SLs, we observed that AO-labeled spots underwent fusion with the plasma membrane by using total internal reflection fluorescence microscopy (Fig. 3*d*).

The total number of visible fluorescence spots was counted to be 61 ± 4 (n = 16) in resting NK cells, corresponding to a total C_m increase of ≈480 fF if all undergo exocytosis. This number is not vastly different from the measured values in microperfusion experiments. PEC stimulation dramatically increased the total number of SLs to 202 ± 12 (n = 16) within 10 min (Fig. 4), a >3-fold increase similar to that observed with C_m measurements (Fig. 2). The result suggests that target-cell recognition augments exocytosis of NK cells by initiating rapid formation of nascent SLs. Our exocytosis assay has demonstrated that these nascent SLs are capable of Ca^{2+}-dependent exocytosis, suggesting that they are formed from a yet-to-be-identified intracellular compartment, which itself is unable to fuse with the plasma membrane. This rapid (<10-min) and dramatic (>3-fold) biogenesis of secretory granules was unexpected, because NK cells

are thought to function through preformed SLs without prior sensitization (6). *De novo* formation of SLs has been suggested for cytotoxic T lymphocytes, because resting T lymphocytes contain no SLs. However, the biogenesis of SLs for cytotoxic T lymphocytes usually takes several days to complete (27), too slow to be compared with the speed found in this study. Rapid biogenesis of secretory organelles is not crucial for the exocytotic function in specialized secretory cells or even other SL-containing hematopoietic cells such as mast cells, neutrophils, etc. These cells usually contain many thousands of preformed secretory organelles, and only a small portion of them are exocytosed after stimulation.

It has been reported that PKC plays vital roles in the exocytosis of NK cells (28). We sought to determine whether PKC is involved in the rapid biogenesis of SLs in NK cells. Preincubation with Gö6983 (1 μM), a specific PKC inhibitor, for 10 min abolished the PEC-induced increase in the total number of SLs, as shown in Fig. 4. On the other hand, treatment with BFA, a fungal metabolite known to inhibit vesicle budding from the TGN (29), did not block the rapid biogenesis of SLs stimulated by PEC (Fig. 4). To further confirm the involvement of PKC in the *de novo* biogenesis of SLs, we challenged NK cells with the PKC activator PMA. As shown in Fig. 4, 100 nM PMA treatment for 5 min significantly increased the number of SLs; however, only a 2-fold increase in the total number of SLs was observed. The effect of PMA was blocked by Gö6983 but not by BFA.

The mechanisms involved in the biogenesis of SLs remain poorly understood. It has been proposed that SLs are generated from the endosomal path (1, 26). However, hematopoietic cells might also directly form SLs from vesicles originating in the TGN (1). Indeed, the acidic feature and presence of both lysosomal and secretory proteins of SLs resemble that of immature granules budded from the TGN (1). It is intriguing to pin down the source of this large amount of vesicular membrane (≈30% of the total cell membrane) generation observed in this study. We have demonstrated that treatment of BFA did not block the rapid *de novo* formation of SLs, suggesting that nascent SLs are not derived from the TGN. Additional work will be necessary to demonstrate whether the nascent SLs are budded from the late endosomes or a yet-uncharacterized structure, i.e., parallel tubular arrays (PTAs) found in human NK cells (30). These PTA granules are suggested as storage organelles for lytic proteins and are thought to transform into lytic granules after target-cell recognition.

Because PKC is activated after target-cell recognition in NK cells, the PKC-mediated rapid budding of SLs found in this study might play an important role in the killing of target cells. It is interesting that abnormal down-regulation of PKC has been suggested to be responsible for the enlargement and reduction in number of lysosomes in a genetic disease called Chediak Higashi syndrome (27, 31). Most cells contain more than one type of fully developed secretory organelles with significant difference in their exocytosis, making the analysis of secretion in those cells complicated. Because NK cells have been suggested to possess only one population of SLs, this study highlights NK cells as an ideal system for investigating the biogenesis, maturation, and exocytosis of SLs and the underlying mechanisms further.

This work was supported by National Science Foundation of China Grants 30025023, 30270363, and 30130230; the Major State Basic Research Program of the People's Republic of China Grants 2001CBS10008 and 2004CB720000; Knowledge Innovation Program Grant KSCX2-SW-224; the Li Foundation; and the Sinogerman Scientific Center. The laboratory of T.X. belongs to a Partner Group Scheme of the Max Planck Institute for Biophysical Chemistry (Göttingen, Germany).

1. Blott, E. J. & Griffiths, G. M. (2002) *Nat. Rev. Mol. Cell Biol.* **3,** 122–131.
2. Sorensen, J. B. (2004) *Pflügers Arch.* **448,** 347–362.
3. Clark, R. & Griffiths, G. M. (2003) *Curr. Opin. Immunol.* **15,** 516–521.
4. Olsen, I., Bou-Gharios, G. & Abraham, D. (1990) *Eur. J. Immunol.* **20,** 2161–2170.
5. Podack, E. R. & Kupfer, A. (1991) *Annu. Rev. Cell Biol.* **7,** 479–504.
6. Stinchcombe, J. C. & Griffiths, G. M. (1999) *J. Cell Biol.* **147,** 1–6.
7. Xu, T., Naraghi, M., Kang, H. & Neher, E. (1997) *Biophys. J.* **73,** 532–545.
8. Grynkiewicz, G., Poenie, M. & Tsien, R. Y. (1985) *J. Biol. Chem.* **260,** 3440–3450.
9. Xia, S., Xu, L., Bai, L., Xu, Z. Q. & Xu, T. (2004) *Brain Res.* **997,** 159–164.
10. Conchello, J. A. & McNally, J. G. (1996) *Preceedings of the 1996 IS&T/SPIE Symposium on Electronic Imaging: Science and Technology,* 199–208.
11. Llopis, J., McCaffery, J. M., Miyawaki, A., Farquhar, M. G. & Tsien, R. Y. (1998) *Proc. Natl. Acad. Sci. USA* **95,** 6803–6808.
12. Neher, E. & Marty, A. (1982) *Proc. Natl. Acad. Sci. USA* **79,** 6712–6716.
13. Gong, J. H., Maki, G. & Klingemann, H. G. (1994) *Leukemia* **8,** 652–658.
14. Oberhauser, A. F., Monck, J. R., Balch, W. E. & Fernandez, J. M. (1992) *Nature* **360,** 270–273.
15. Nusse, O. & Lindau, M. (1988) *J. Cell Biol.* **107,** 2117–2123.
16. Nusse, O., Serrander, L., Lew, D. P. & Krause, K. H. (1998) *EMBO J.* **17,** 1279–1288.
17. Sadahira, Y., Akisada, K., Sugihara, T., Hata, S., Uehira, K., Muraki, N. & Manabe, T. (2001) *Virchows Arch.* **438,** 280–288.
18. Cole, K. S. (1968) *Membranes, Ions and Impulses* (Univ. of California Press, Berkeley).
19. Alvarez de Toledo, G. & Fernandez, J. M. (1990) *J. Cell Biol.* **110,** 1033–1039.
20. Baumann, B. C., Forte, P., Hawley, R. J., Rieben, R., Schneider, M. K. & Seebach, J. D. (2004) *J. Immunol.* **172,** 6460–6467.
21. Neher, E. & Zucker, R. S. (1993) *Neuron* **10,** 21–30.
22. Xu, T., Binz, T., Niemann, H. & Neher, E. (1998) *Nat. Neurosci.* **1,** 192–200.
23. Voets, T. (2000) *Neuron* **28,** 537–545.
24. Smith, C., Moser, T., Xu, T. & Neher, E. (1998) *Neuron* **20,** 1243–1253.
25. Swanson, M. L. & Pessin, J. E. (1989) *J. Membr. Biol.* **108,** 217–225.
26. Burkhardt, J. K., Hester, S., Lapham, C. K. & Argon, Y. (1990) *J. Cell Biol.* **111,** 2327–2340.
27. Stinchcombe, J. C., Page, L. J. & Griffiths, G. M. (2000) *Traffic* **1,** 435–444.
28. Leibson, P. J., Midthun, D. E., Windebank, K. P. & Abraham, R. T. (1990) *J. Immunol.* **145,** 1498–1504.
29. Lippincott-Schwartz, J., Donaldson, J. G., Schweizer, A., Berger, E. G., Hauri, H. P., Yuan, L. C. & Klausner, R. D. (1990) *Cell* **60,** 821–836.
30. Kolb, S. A. & Groscurth, P. (1997) *Anat. Embryol.* **196,** 215–226.
31. Tanabe, F., Cui, S. H. & Ito, M. (2000) *J. Leukocyte Biol.* **67,** 749–755.